Ab initio quantum mechanical modeling of infrared vibrational frequencies of the OH group in dioctahedral phyllosilicates. Part II: Main physical factors governing the OH vibrations

Sara Martínez-Alonso,[1,2,*] James R. Rustad,[3] and Alexander F.H. Goetz[1,2]

[1]Department of Geological Sciences, University of Colorado at Boulder, Boulder, Colorado 80309-0399, U.S.A.
[2]Center for the Study of Earth from Space, Cooperative Institute for Research in Environmental Sciences, Boulder, Colorado 80309-0216, U.S.A.
[3]W.R. Wiley Environmental Molecular Sciences Laboratory, Pacific Northwest National Laboratory, Richland, Washington 99352, U.S.A.

Abstract

The physical factors responsible for the variability observed in OH infrared (IR) fundamentals in dioctahedral phyllosilicates, due to octahedral substitution of Al^{3+} by Mg^{2+}, Fe^{2+}, and Fe^{3+}, are discussed here. The data analyzed consist of experimental frequencies as well as frequencies modeled using Density Functional Theory (DFT) calculations.

The charge of the octahedral cations surrounding the OH is one of the main factors affecting both the OH stretch and the in-plane bend; cationic electronegativity and ionic radius play important roles in the stretch and bend modes, respectively. The mass of the octahedral cations does not affect the OH fundamental vibrations.

The nature of the octahedral cations alone can explain most of the variability observed in the OH in-plane bend, making this fundamental vibration the most suitable for assessing octahedral composition. Discrepancies between modeled and experimental OH stretch frequencies indicate the existence of other factors governing this fundamental vibration. Further DFT calculations indicate that apical O atoms of the tetrahedral sheet with unsatisfied charges due to octahedral and/or tetrahedral substitutions can explain these discrepancies.

The modeling results are utilized to predict the frequency of the OH stretch and in-plane-bend combination band that occurs near 4545 cm^{-1} (2.2 μm) in phyllosilicates. This band can be observed in imaging spectrometer data, allowing for the detection and analysis of phyllosilicates and other minerals in large natural systems. The modeling results confirm that the variability observed in the combination band of dioctahedral phyllosilicates reflects octahedral and, to a certain degree, tetrahedral composition, but not interlayer composition.

Introduction

The interactions between octahedral cations and neighboring hydroxyl groups are responsible for the most characteristic absorption features observed in the infrared (IR) spectra of phyllosilicates. As a consequence, the nature of the octahedral cations can be inferred from spectroscopic studies (Ŝtubiĉan and Roy 1961; Farmer 1974 and references herein; Clark et al. 1990; Petit et al. 1999; Yang et al. 2001). However, the physical mechanisms that govern the OH fundamental vibrations observed experimentally are not yet fully understood.

For the simple case of a two-atom system, the vibrational frequency (ν), derived from the quantum mechanical treatment of the harmonic oscillator, is a function of the bond force constant (*k*) and the reduced mass of the system (μ):

$$v = \frac{1}{2\pi}\sqrt{\frac{k}{\mu}} \qquad (1)$$

Force constants reflect the strength of the bonds between atoms, and they represent a balance between nuclear repulsions, electron repulsions, and electron-nuclear attractions (Hollas 1996). Each of the $3n$-6 possible modes of vibration in a nonlinear molecule encompassing *n* atoms (or $3n$-5 modes in a linear molecule) has its own associated force constant. Various parameters influence the value of the force constant of each mode, and, thus, its vibrational frequency.

The fundamental vibrational frequencies of the OH group in various dioctahedral environments were modeled using Density Functional Theory (DFT) ab initio quantum mechanical calculations and compared to experimental data, as described in detail in Martínez-Alonso et al. (2002). The modeling approach used in this study allows us to isolate and analyze the physical parameters responsible for the variability observed in the IR spectra of phyllosilicate samples. We focus on the analysis of the OH stretch [ν(OH)] and in-plane bend [δ(OH)] fundamental vibrations because their combination mode can be studied using imaging spectrometer remote sensing data. Unlike the OH fundamental vibrations, this 2.2 μm combination band can be observed in reflected imaging spectrometer data, as it occurs in an atmospheric transmission window: a portion

* Present address: Laboratory for Atmospheric and Space Physics, University of Colorado, Boulder, CO 80309-0392, U.S.A. E-mail: martinas@lasp.colorado.edu

of the electromagnetic spectrum in which the absorption of incoming solar irradiance by atmospheric gases is minimal. Imaging spectrometers allow for the identification of mineral species and also for the detection of subtle chemical variations in their composition in large natural systems. Very detailed mineralogical maps of extensive regions can now be derived from imaging spectrometer data, unveiling spatial patterns that help clarify genetic processes, alteration zoning, and sediment transportation vectors, among others.

PREVIOUS MODELS EXPLAINING THE OH FUNDAMENTAL FREQUENCIES

Several (sometimes opposed) models have been proposed to rationalize the main physical factors responsible for the variability observed in the ν(OH) in phyllosilicates (Vedder 1964; Velde 1983; Robert and Kodama 1988; Besson and Drits 1997b; Sainz-Díaz et al. 2000), as well as in the δ(OH) (Sainz-Díaz et al. 2000).

From the study of IR data obtained from di- and trioctahedral phyllosilicates, Vedder (1964) hypothesized an inverse relationship between ν(OH) frequency and octahedral cationic charge, consistent with Equation 1. According to this model, octahedral cations with high positive charge next to the hydroxyl group would decrease the strength of the O-H bond and therefore decrease its ν(OH) frequency.

However, new IR data of natural minerals presented by Slonimskaya et al. (1986), as well as IR data for synthetic phyllosilicates obtained by Velde (1978), conflict with the model proposed by Vedder. From the analysis of experimental data of hydrous silicates, Velde (1983) concluded that both charge and electronegativity of the octahedral cations surrounding the OH could explain the ν(OH) band positions. An increase in charge and electronegativity would correspond to a decrease in the ν(OH) frequency.

Robert and Kodama (1988) found that the relationship between octahedral charge and ν(OH) frequency was in fact the opposite of that identified by Vedder (1964). They proposed a new model explaining the positions of the ν(OH) bands observed in both tri- and dioctahedral phyllosilicates. According to their model, the ν(OH) frequency is not only influenced by the charge of the nearest octahedral cations, but also, and more strongly, by neighboring tetrahedral apical O atoms with unsatisfied charges. Al^{3+} for Si^{4+} substitutions in the tetrahedral sheet and Mg^{2+} for Al^{3+} substitutions or vacancies in the octahedral sheet produce local charge imbalances in the tetrahedral apical O atoms, which then interact with the H atom in the hydroxyl groups, weakening the OH bond and lowering the ν(OH) frequency. According to this model, it would not be possible to characterize a mica (phyllosilicate) phase by its ν(OH) frequencies because of the overlapping effects caused by tetrahedral and octahedral substitution.

Besson and Drits (1997a) studied a suite of dioctahedral phyllosilicate samples, and were able to differentiate pyrophyllite-like (without neither tetrahedral nor octahedral charge) from muscovite-like local structural environments, according to their ν(OH). They also showed that, for different dioctahedral phyllosilicate samples with the same local structural environment, the ν(OH) frequencies corresponding to the same octahedral cationic environment were always within ± 3 cm^{-1}.

Besson and Drits (1997b) proposed a new model, applicable to dioctahedral phyllosilicates, according to which the main factor responsible for the stretch frequencies of an OH group is the nature (charge and atomic mass) of the octahedral cations to which it is coordinated, and, to a lesser degree, the nature of the octahedral and tetrahedral cations surrounding the nearby apical O atoms.

Sainz-Díaz et al. (2000) used Hartree-Fock ab initio quantum mechanical calculations to model the octahedral cation-OH interaction, and concluded that both the mass of the octahedral cations and electron density distribution, estimated through Mulliken population analysis, affect the ν(OH) and δ(OH) fundamentals. By comparison to experimental data, these authors concluded that the ν(OH) in clays is also influenced by tetrahedral apical O atoms, and by substitution of Si by Al in the tetrahedral sheet.

PHYSICAL FACTORS CONTROLLING THE OH FUNDAMENTAL VIBRATIONS

The fundamental modes of vibration of two atomic models labeled Small Dimer and Dimer clusters, representing the OH group and its immediate octahedral environment, at the DFT/DND level of theory have been calculated (Martínez-Alonso et al. 2002). The Small Dimer consists of two octahedral cations and two hydroxyl groups: [MM'(OH)$_2$], where MM' = Al^{3+}, Mg^{2+}, Fe^{2+}, and Fe^{3+}. The Dimer cluster [MM'(OH)$_2$(H$_2$O)$_8$] evolves from the Small Dimer by adding water molecules coordinated to the MM' cations, to complete their coordination shell.

A discussion follows on the role of various physical mechanisms (charge, electronegativity, ionic radii, and atomic mass of the octahedral cations, summarized in Table 1), which could be responsible for the OH fundamentals modeled and observed experimentally.

Effects of charge of the octahedral cations

According to the modeling results shown in Figures 1 and 2, the charge of the octahedral cations appears to be an important factor controlling the ν(OH) frequencies in the clusters modeled: the wavenumbers increase as the octahedral charge surrounding the OH group decreases. It can also be observed in Figure 3 that the O-H bond distance is highly correlated with

TABLE 1. Some characteristic parameters of the MM' octahedral cation arrangements in the clusters modeled

MM'	Average charge	Average mass (amu)	Ionic radius (Å) *	EN †	IP ‡
Fe$_2^{3+}$	3.0	55.847	0.650	1.83	4.61
Fe^{3+}Al	3.0	41.414	0.590	1.72	5.14
Al$_2$	3.0	26.982	0.530	1.61	5.66
Fe^{2+}Fe^{3+}	2.5	55.847	0.710	1.83	3.61
MgFe^{3+}	2.5	40.076	0.685	1.57	3.70
AlFe^{2+}	2.5	41.414	0.650	1.72	4.13
AlMg	2.5	25.643	0.625	1.46	4.22
Fe$_2^{2+}$	2.0	55.847	0.770	1.83	2.60
MgFe^{2+}	2.0	40.076	0.745	1.57	2.69
Mg$_2^{2+}$	2.0	24.305	0.720	1.31	2.78
Sr$_2^{2+}$	2.0	87.620	1.16	0.95	1.72
Be$_2^{2+}$	2.0	9.012	0.35	1.57	5.71

* Average ionic radii from Shannon and Prewitt (1969). High spin configuration radii for Fe^{2+} and Fe^{3+} were utilized.
† Average electronegativities (EN) are given in the Pauling scale.
‡ Average Ionic Potential (IP) is the mean of the ratios between charge and ionic radius for each MM' metal.
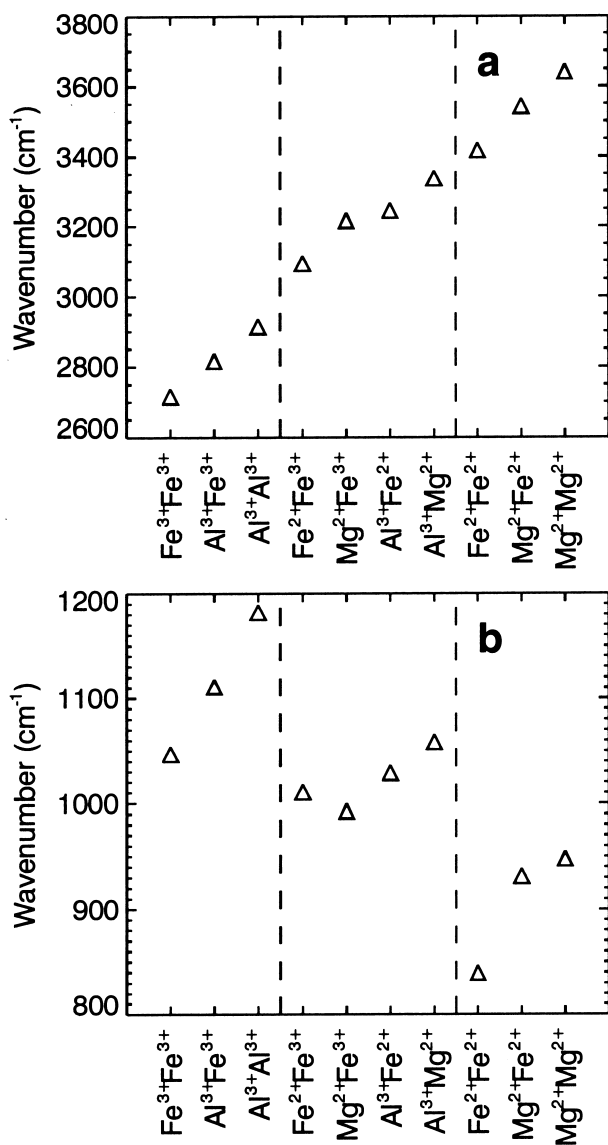
FIGURE 1. Summary of non-scaled wavenumbers calculated for the Small Dimers: ν(OH) (**a**), and δ(OH) (**b**). Dashed lines separate cationic groups with the same total charge. Octahedral cations are arranged by decreasing charge and, within groups with the same charge, by decreasing electronegativity.

FIGURE 2. Summary of non-scaled wavenumbers calculated with the DFT/DND model for the Dimer clusters: ν(OH) (**a**), and δ(OH) (**b**). Dashed lines separate cationic groups with the same total charge. Octahedral cations are arranged by decreasing charge and, within groups with the same charge, by decreasing electronegativity.

the ν(OH) wavenumber, as expected. This agrees with Badger's rule, an empirical expression that allows the prediction of internuclear distances of polyatomic molecules from vibrational data with considerable accuracy (Badger 1934, 1935). If the charge of the metal is large, the O atoms bonded to it become strongly polarized: their electrons are pulled closer to the metals, and a decreased electron density is available to bind the hydrogen atom. As a consequence, the OH bond grows longer and weaker, which translates into a smaller bond force constant. This leads to lower ν(OH) frequencies, as shown by Equation 1. If the charge of the metal is low, the OH bond will be shorter and stronger, leading to higher ν(OH) frequencies.

There is less variability in the ν(OH) frequencies and OH

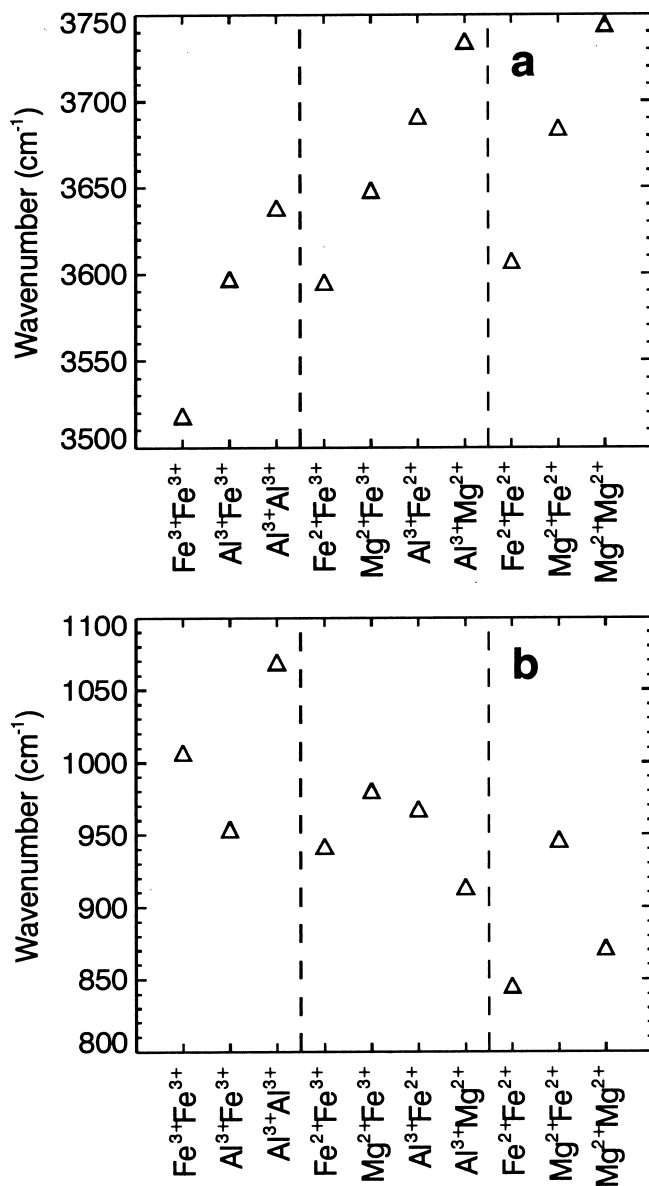bond lengths in the Dimer clusters than in the Small Dimers, since the electron-density around the metals is increased by the presence of water molecules. This is further evidence of the dependence of the ν(OH) frequency on the charge of the octahedral metals.

In Figures 1 and 2 we showed that the δ(OH) frequencies decrease with decreasing metal charge. The charge affects the δ(OH) frequency in the following manner: as stated above, a large cationic charge strongly polarizes the O atoms. This means that the O atom's lone pairs are more tightly coordinated to the metals, therefore the OH group is "anchored" by the metal centers, and its bending motion is restricted. This translates to a higher δ(OH) frequency.
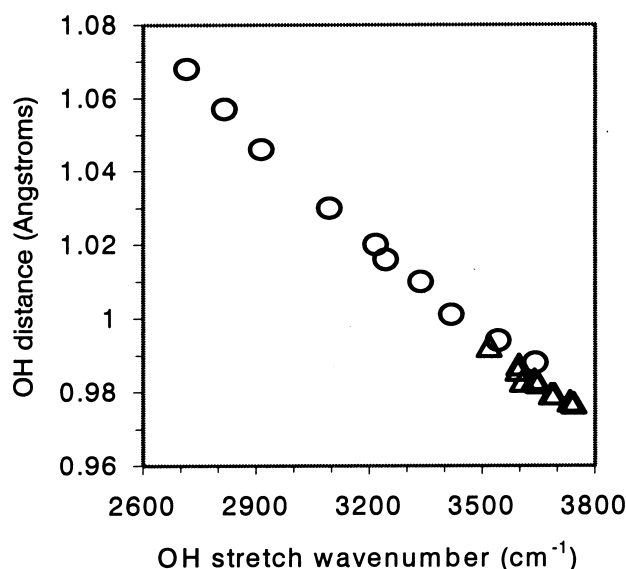
FIGURE 3. DFT/DND non-scaled modeled ν(OH) wavenumbers vs. modeled length of the OH bond. Circles = small dimers; triangles = dimers.

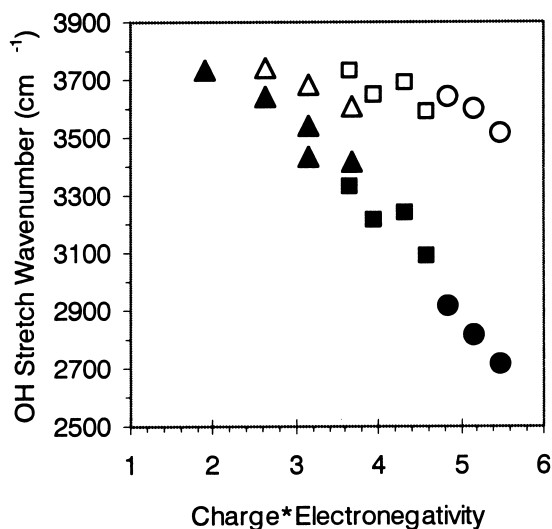**FIGURE 4.** DFT/DND non-scaled modeled ν(OH) wavenumbers vs. the product of average electronegativity and average charge of the MM' octahedral cations. Filled figures = small dimers (including Be^{2+} and Sr^{2+}); open figures = dimers; circles = $M^{3+}M^{3+}$; squares = $M^{3+}M^{2+}$; triangles = $M^{2+}M^{2+}$.

Effects of electronegativity of the octahedral cations

Several authors have found a negative correlation between experimental band positions of ν(OH) in hydrous silicates and the electronegativity of the surrounding cations (Wilkins and Ito 1967; Strens 1974; Velde 1983). We find the same relationship in our modeling results for the Small Dimers and Dimers clusters. The negative correlation is made even more evident by including the effect of octahedral charge. Figure 4 shows the product between electronegativity and charge of the metals vs. calculated ν(OH) wavenumber. A decrease of the slopes defined by the data points can be observed from Small Dimers to Dimers. This can be explained by the decrease in charge of the metals available to interact with the hydroxyl groups.

Electronegativity is a valuable guide to understanding bond character. The difference between the electronegativities of two bonded atoms gives us an idea of the degree of ionic character of that bond. It is generally accepted that the octahedral cation-O atom (M-O) bond is mostly ionic (Iishi 1978; Hill et al. 1979). Nevertheless, the ionic character of this bond varies between 50% (Fe-O bond), 60% (Al-O bond), and 65% (Mg-O bond) (Gill 1989), that is, it increases as the electronegativity of the cation decreases. In a strongly ionic bond, the valence electrons of the less electronegative atom will be drawn from their orbitals to complete the valence orbitals of the more electronegative atom. The O atom will have more electron density available to bind the hydrogen atom. As a consequence, the OH bond will be shorter and the ν(OH) frequency higher. The less ionic the M-O bond, the more polarized the O atom's electrons will be toward the cation M. Longer OH bonds and lower ν(OH) frequencies will be the result.

To test the hypothesis that increasing electronegativity of the octahedral cations reduces the frequency of ν(OH), two new Small Dimers {$[Be_2^{2+}(OH)_2]^{2+}$ and $[Sr_2^{2+}(OH)_2]^{2+}$} were modeled at the DFT/DND level of theory. Be and Sr were selected because among divalent cations they have quite extreme electronegativities: $E°(Be) = 1.57$, whereas $E°(Sr) = 0.95$. Stron-

tium producing the most ionic bond with the O should present the shortest OH bond and the highest ν(OH) frequency. The Be-O bond's ionic character is between those of the Mg-O and Fe^{2+}-O bonds, as should the Be-related OH bond length and ν(OH) frequency. Modeling results confirm the expected relationships between the ionic character of the M-O bond and ν(OH) frequency [see Table 4 in Martínez-Alonso et al. (2002) for a comparison with the other Small Dimer results]. The calculated ν(OH) wavenumbers for $[Be_2^{2+}(OH)_2]^{2+}$ and $[Sr_2^{2+}(OH)_2]^{2+}$ are 3433 and 3731 cm^{-1}, respectively. The O-H distances for the same two models are 1.001 and 0.978 Å.

For equally charged metals, we see in the δ(OH) frequencies approximately the same secondary trend as in the ν(OH) frequencies. This trend cannot be explained by the electronegativity of the metals, since electronegativity would have an effect on the bending frequencies opposite to that on the stretching frequencies. Metals with larger electronegativity would polarize the O atoms more. As was discussed above, a stronger polarization of the O atoms translates into a higher bending frequency. The results calculated for the Sr^{2+} and Be^{2+} models confirm this point: the bending frequency calculated for Sr^{2+}, the cation with the lowest electronegativity, is the lowest among those of the divalent cations (802 cm^{-1}), whilst that of Be^{2+} is the highest (1025 cm^{-1}).

Electronegativity can thus explain the secondary trend observed in the ν(OH) fundamental among equally charged clusters, but not that observed in the δ(OH).

Effects of mass of the octahedral cations

Atomic mass of the neighboring octahedral cations has commonly been considered one of the main factors affecting the sequence of ν(OH) positions observed experimentally (Wilkins and Ito 1967; Brindley and Kao 1984; Slonimskaya et al. 1986; Besson and Drits 1997a, 1997b; Sainz-Díaz et al. 2000). Cationic

mass would affect the OH vibrational frequencies only if coupling between vibrations of the cations and the ν(OH) occurred.

As Velde (1983) stated, "since atomic mass and electronegativity are roughly correlated […], it is difficult to distinguish, initially, between the two factors". To test the hypothesis that atomic mass of the octahedral cations affects the ν(OH) frequency, vibrational frequencies were calculated at the Hartree-Fock level of theory[1], using a Triple Zeta Valence (TZV) basis set for a $[Al_2(OH)_2]^{4+}$ Small Dimer cluster in which the cationic sites were occupied by Al atoms to which the mass of Fe (55.84 amu) was assigned. The results were then compared with frequencies calculated using the same technique for a $[Al_2(OH)_2]^{4+}$ Small Dimer cluster in which the Al atoms were assigned their actual mass (26.98 amu). The results of both calculations are shown in Table 2. Whereas the frequencies of the fundamentals involving motion of the Al atoms were influenced by this mass change (increasing the Al atoms mass decreased their frequency), the OH fundamentals remained unchanged. This result supports the assumption that ν(OH) is not strongly coupled to the M-O stretch, and therefore, the mass of the neighboring octahedral cations does not affect the OH vibrational frequencies.

Effects of ionic radii of the octahedral cations

Ionic radii of the octahedral cations could influence the OH bond in the following manner: for equal cationic charge, a smaller cation could place its charge closer to the O atom, and, therefore, polarize it more strongly. We can combine charge and ionic radii into ionic potential, the ratio of the cation's charge to its radius. The ionic potential of a cation is a measure of its power to polarize an anion and recover a fraction of the excess electron density (Gill 1989).

Figure 5 shows a strong positive correlation between the calculated δ(OH) wavenumber and the ionic potential of the metals. This figure includes data points for the $[Be_2^{2+}(OH)_2]^{2+}$ and $[Sr_2^{2+}(OH)_2]^{2+}$ clusters. Be and Sr have extreme ionic radii among divalent cations: 0.35 Å for Be and 1.16 Å for Sr. As stated above, for equally charged metals, the smaller the ionic radii, the more they will polarize the O atoms, thus increasing the δ(OH) frequency. Consequently, charge and ionic radius combined as ionic potential could explain the secondary trend observed in δ(OH).

The secondary trend observed in modeled ν(OH) frequencies is opposite to the expected effect of cationic ionic radii. For equal cationic charge, smaller cations would produce longer, weaker OH bonds and consequently lower ν(OH) frequencies for smaller metals. This was confirmed by analyzing the equilibrium geometry and vibrational frequencies calculated for the $[Be_2^{2+}(OH)_2]^{2+}$ and $[Sr_2^{2+}(OH)_2]^{2+}$ Small Dimer clusters, and comparing the results to those of the other Small Dimers with divalent cations. For Be, the calculated OH bond distance was equal to the largest among the Small Dimers with divalent cations, and the ν(OH) wavenumber was close to the lowest. For Sr, the OH bond length was the shortest and the ν(OH) wavenumber

---

[1]The HF method was applied for these particular calculations because, unlike the DFT software available to us, it allows for isotopic substitutions.

the highest. This shows that for equally charged molecules, smaller cations would lower the ν(OH) frequency. This effect may be overpowered by the opposite effect caused by cationic electronegativity.

Effects of apical O atoms from the tetrahedral sheet

Discrepancies between modeling and experimental results in the case of ν(OH) in dioctahedral environments (Fig. 6) point to the existence of factors other than the nature of the neighboring octahedral cations affecting this fundamental vibration (Martínez-Alonso et al. 2002). Whilst theory predicts an increase in the ν(OH) frequency as the charge of the neighboring cations decreases, experimental data shows a slight decrease instead.

Experimental OH frequencies of trioctahedral phyllosilicates and actinolites (whose structure at large scale very closely resembles that of trioctahedral phyllosilicates) show an increase in ν(OH) frequency with decreasing octahedral charge predicted through modeling (Fig. 7). This would indicate that, unlike in dioctahedral minerals, the frequency of the ν(OH) vibration in
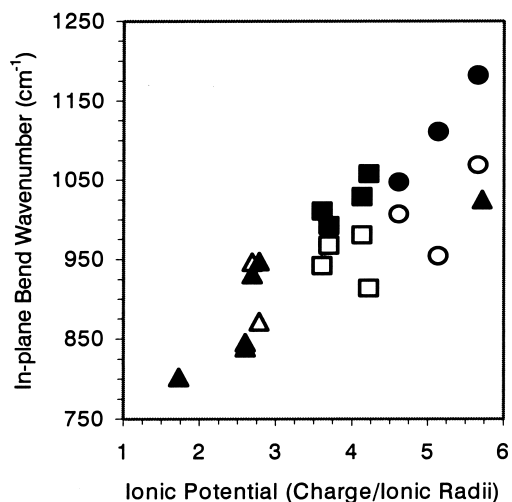
FIGURE 5. Non-scaled calculated δ(OH) wavenumber vs. ionic potential of the octahedral cations surrounding the OH. Filled figures = small dimers; open figures = dimers; circles = $M^{3+}M^{3+}$; squares = $M^{3+}M^{2+}$; triangles = $M^{2+}M^{2+}$.

TABLE 2. Non-scaled wavenumbers calculated at the HF/TZV level of theory for two $Al_2(OH)_2$ clusters

Fundamental	Wavenumber (cm^{-1})	
	$Al_2(OH)_2$ (m_{Al} = 26.98 amu)	$Al_2(OH)_2$ (m_{Al} = 55.84 amu)
Symmetric ν(OH)	3589	3589
Asymmetric ν(OH)	3567	3567
Symmetric δ(OH)	1414	1413
Asymmetric δ(OH)	1410	1406
Symmetric OH out-of-plane bend	965	958
Asymmetric OH out-of-plane bend	895	895
Symmetric Al-OH stretch	772	756
Asymmetric Al-OH stretch	699	625
Symmetric Al-OH in-plane bend	659	590
Asymmetric Al-OH in-plane bend	539	493
Al-Al stretch	503	357
Al-OH out-of-plane bend	330	297

Note: In the first cluster the Al atoms have their actual mass (26.98 amu.); in the second, the mass of Fe (55.84 amu) has been assigned to the Al atoms.

trioctahedral environments can be mostly explained by the nature of the octahedral cations surrounding the OH group.

Due to the different occupancy of the octahedral cationic sites, the OH vector has different orientation in tri- and dioctahedral environments. In general, all the octahedral sites are occupied by divalent cations in trioctahedral minerals. Therefore, the O atom in the OH group is bonded to three neighbor cations through tetrahedral hybrid sp^3 orbitals and the hydrogen atom has to lie along the fourth sp^3 orbital which has to be equally inclined respect to the other three (Saksena 1964), that is, roughly perpendicular to the sheets. In dioctahedral minerals, one of the three cationic sites near the OH group is vacant and the other two are most commonly occupied by trivalent cations. In this type of environment, the OH vector is inclined toward the vacancy, and away from the two occupied sites (approximately parallel to the sheets). In dioctahedral phyllosilicates the OH inclination brings the hydrogen atom closer to two of the apical O atoms from the tetrahedral sheet, forming bonds between the hydrogen atom and these O atoms (Saksena 1964; Farmer 1974; Besson and Drits 1997b).

Interaction of the hydroxyl group with unsatisfied apical O atoms from the tetrahedral sheet could be the factor responsible for the discrepancies we observed between experimental and modeling results in dioctahedral environments. If divalent cations occupy the dioctahedral sites, then part of the charge of the apical O atoms will be unsatisfied. This charge will act upon the H atom, increasing the OH distance and lowering the stretch frequency. Substitution of Si^{4+} by Al^{3+} in the tetrahedral sheet would produce identical results. Experimental ν(OH) wavenumbers in pyrophyllite-like environments can be clearly distinguished from those in muscovite-like environments, as

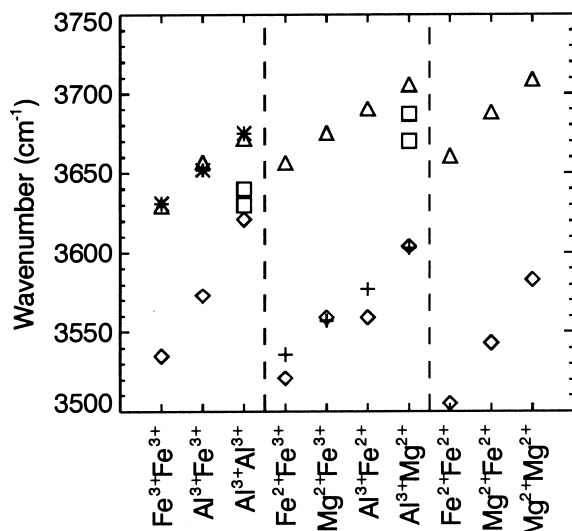pointed out by Besson and Drits (1997a). In mica-like environments, the tetrahedral sheet charge caused by the presence of trivalent cations lowers the ν(OH) wavenumbers. Smectites, with fewer tetrahedral substitutions than muscovite, have ν(OH) values intermediate between those of pyrophyllite- and muscovite-like environments (Fig. 6).

To assess the effect on the ν(OH) frequency of the OH vector orientation and proximity to apical O atoms with satisfied or unsatisfied charges, a new modeling scheme was needed. In this case, the OH orientation had to be fixed to keep its position relative to the octahedral cations and apical O atoms. Therefore, a traditional frequency calculation on the Small Dimers and Dimers with full optimization of the cluster's geometry was not possible, because it would lead to hydroxyl groups being coplanar with the octahedral cations. Surrounding the $[MM'(OH)_2]$ unit by its first solvation shell and capping hydrogen atoms to lower the total charge (a 106-atom cluster), and constraining the geometry of all the atoms except for the OH group and octahedral cations would lead to the proper OH orientation, as shown by PM3(tm) semi-empirical calculations performed in this study. Nevertheless, a complete DFT calculation on a 106-atoms molecule would be impractical with the computers presently available to the authors. The use of semi-empirical methods for frequency calculations was discarded because of insufficient accuracy of the results they provide (Martínez-Alonso et al. 2002). Instead, DFT Single Point Energy Calculations (SPEC) were performed. SPEC consists of calculating the energy corresponding to a cluster whose geometric configuration is constrained. By obtaining SPEC results for identical clusters where only the OH distance is modified
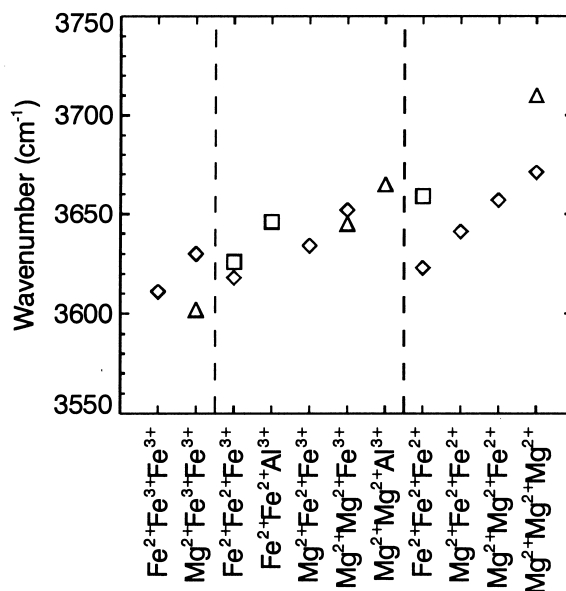

FIGURE 6. Experimental ν(OH) wavenumbers in dioctahedral environments compiled from Farmer (1974) for smectites (squares) and celadonites (crosses), and Besson and Drits (1997a) for pyrophyllite-like (asterisks) and muscovite-like (circles) environments. Modeled, scaled wavenumbers for the Dimers are also shown for comparison (filled diamonds). Dashed lines separate cationic groups with the same total charge. Octahedral cations are arranged by decreasing charge and, within groups with the same charge, by decreasing electronegativity.

FIGURE 7. Experimental ν(OH) wavenumbers in trioctahedral environments. Squares = synthetic trioctahedral micas (Redhammer et al. 2000); diamonds = actinolites (Burns and Greaves 1971); triangles = natural trioctahedral micas (Farmer 1974). Dashed lines separate cationic groups with same charge. Octahedral cations are arranged by decreasing charge and, within groups with the same charge, by decreasing electronegativity.

(simulating its behavior during the stretch motion), a Potential Energy Surface (PES) curve can be constructed, the second derivative of its minimum calculated, and the stretch frequency of the OH group determined. The clusters modeled were slightly modified Dimers (based on atomic coordinates published by Rothbauer 1971), in which the OH vector is oriented in a similar way as it would be in a natural muscovite, inclined approximately 15° with respect to the sheets (Besson and Drits 1997b). Because of its orientation, each OH group is closest to two apical O atoms from the tetrahedral sheet, which form hydrogen bonds with the hydrogen atom in the hydroxyl group (Besson and Drits 1997b, and references therein). Because they are surrounding an octahedral vacancy, these apical O atoms have unsatisfied negative charge. Only one of the two closest apical O atoms per OH group has been included in the modified Dimers. By including both, we would only amplify the effect that we observe with one.

In a first set of SPEC experiments, no apical O atoms were included. In a second set, two apical O atoms with unsatisfied charges were added (Fig. 8). In a third set of experiments, the charges of the two apical O atoms were satisfied via coordination with hydrogen atoms. These SPEC experiments were repeated for Al_2, AlMg, and Mg_2 modified Dimers. The calculated energies, PES minimum, second derivatives of the PES at its minimum, and stretch wavenumbers for all the modified Dimers are shown in Table 3.

By changing the orientation of the OH vector (SPEC experiment with no apical O atoms), the relative trend between ν(OH) frequencies in the modified Dimers remains the same as for the Dimer clusters: the Al_2 cluster still presents the lowest frequency. Changing the OH vector orientation and including apical O atoms with satisfied charges does not lower the ν(OH) frequency of the Mg_2 or AlMg clusters below the ν(OH) frequency of the Al_2 cluster without apical O atoms or with satisfied apical O atoms. Only if the apical O atoms near the Mg_2 or AlMg clusters have unsatisfied charges are their ν(OH) frequencies below the frequency of the Al_2 cluster both without apical O atoms and with satisfied apical O atoms.

From these results we can conclude that in dioctahedral minerals both the nature of the neighboring octahedral cations and the interaction with unsatisfied apical O atoms of the tetrahedral sheet play important roles in determining the frequency of ν(OH). This is in agreement with the model proposed by Robert and Kodama (1988).

The composition of the tetrahedral sheet produces a considerable effect on the ν(OH), through unbalanced charges and probably through subsequent distortions of the crystalline structure. Both effects (direct effect of octahedral cations and indirect effect of apical O atoms) overlap, and it is not possible to differentiate between the two by studying the vibrations of hydroxyl alone. Additional information on tetrahedral cationic (T) composition could be retrieved by analyzing IR spectra in the 700–1200 cm^{-1} region (to detect T-O stretching frequencies) and 150–600 cm^{-1} region (T-O bending).

THE ν(OH) AND δ(OH) COMBINATION BAND

Vedder and McDonald (1963) identified the combination of ν(OH) and δ(OH) occurring near 4542 cm^{-1} (2.2 μm). From
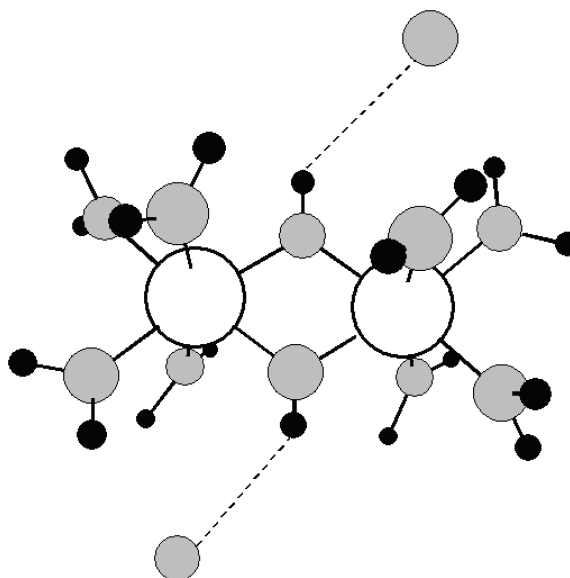

FIGURE 8. Modified Dimer with tetrahedral apical O atoms used in the SPEC modeling experiment. OH vectors are oriented in the same way as they are in muscovite and two apical O atoms from the tetrahedral sheet have been included. Open circles = octahedral cations; gray circles = O atoms; black circles = hydrogen atoms.

early on, the remote sensing community has paid special attention to this combination band as an indicator of the composition of phyllosilicate minerals. Hunt and Salisbury (1970) and Hunt et al. (1973) recognized different locations of the OH combination band in phyllosilicates, according to their octahedral composition. Numerous studies relating the near IR spectra of phyllosilicates and their compositions followed (Post and Noble 1993; Duke 1994; Swayze 1997; Bishop et al. 1999; Yang et al. 1999; Madejová 2000).

Experimental data

Short Wave Infrared (SWIR) reflectance spectra of some of the muscovite, illite, and interlayered illite/smectite samples described in Martínez-Alonso et al. (2002) were acquired with an Analytical Spectral Devices-Full Range (ASD-FR) field scanning spectroradiometer for wavelengths between 0.35 and 2.5 μm. The spectral sampling interval of this instrument is 0.0014 μm in the 0.35 to 1.0 μm range, and 0.002 μm in the 1.0 to 2.5 μm range. Its spectral resolution goes from 0.003 μm in the region between 0.35 and 1.0 μm, to 0.01 μm in the spectral region between 1.0 and 2.5 μm. Its spectral accuracy is 0.001 μm. No sample preparation was required.

All the samples analyzed presented a main OH combination band located near 2.2 μm, and in some cases a second OH combination band located on the long wavelength limb of the main one. The OH combination bands were located by visual inspection of continuum-removed spectra. The spectra were divided by the convex hull connecting the local minimum and maximum of the larger absorption band on which the OH combination bands were superimposed (2.14 and 2.27 μm, respectively, for the main band, and 2.22 and 2.27 for the second

TABLE 3. SPEC numerical results for modified Dimer clusters

OH x^*	No apical O			Two O^{2-}			Two O^0		
	E Al$_2$†	E AlMg†	E Mg$_2$†	E Al$_2$†	E AlMg†	E Mg$_2$†	E Al$_2$†	E AlMg†	E Mg$_2$†
0.82	−1239.499	−1197.80	−1155.947	−1389.993	−1347.785	−1305.406	−1391.284	−1349.565	−1307.688
0.84	−1239.517	−1197.821	−1155.965	−1390.013	−1347.804	−1305.425	−1391.303	−1349.584	−1307.706
0.86	−1239.532	−1197.836	−1155.979	−1390.029	−1347.820	−1305.440	−1391.318	−1349.598	−1307.720
0.88	−1239.544	−1197.848	−1155.990	−1390.042	−1347.832	−1305.452	−1391.330	−1349.610	−1307.732
0.9	−1239.553	−1197.856	−1155.999	−1390.052	−1347.842	−1305.461	−1391.339	−1349.619	−1307.740
0.92	−1239.560	−1197.863	−1156.005	−1390.060	−1347.849	−1305.468	−1391.346	−1349.626	−1307.747
0.94	−1239.564	−1197.867	−1156.009	−1390.066	−1347.855	−1305.473	−1391.351	−1349.630	−1307.751
0.96	−1239.567	−1197.869	−1156.011	−1390.070	−1347.858	−1305.476	−1391.354	−1349.633	−1307.753
0.98	−1239.568	−1197.870	−1156.012	−1390.073	−1347.860	−1305.477	−1391.356	−1349.634	−1307.754
1.00	−1239.568	−1197.869	−1156.011	−1390.074	−1347.861	−1305.477	−1391.356	−1349.633	−1307.754
1.02	−1239.566	−1197.868	−1156.010	−1390.075	−1347.860	−1305.476	−1391.355	−1349.632	−1307.752
1.04	−1239.564	−1197.865	−1156.007	−1390.074	−1347.859	−1305.474	−1391.353	−1349.630	−1307.749
1.10	−1239.551	−1197.852	−1155.993	−1390.069	−1347.851	−1305.463	−1391.342	−1349.617	−1307.736
1.20	−1239.520	−1197.819	−1155.959	−1390.052	−1347.828	−1305.436	−1391.312	−1349.586	−1307.703
x_{min} *	0.987	0.98	0.98	1.018	1.0	0.991	0.991	1.0	0.981
d^2E/dx^2 ‡	3.31624	3.45196	3.42137	2.26149	2.751	3.08353	3.15659	3.33157	3.42798
$\bar{v}$ §	4940	5040	5017	4079	4499	4763	4819	4951	5022

* OH distance (x) and minimum OH distance (x_{min}) in angstroms.
† Energy (E) in Hartrees.
‡ d^2E/dx^2 is the second derivative of the PES at its minimum.
§ Wavenumber ($\bar{v}$) in cm^{-1}.

one). The location of the OH combination bands identified in these samples is shown in Table 4.

Comparison between predicted location of the combination band and experimental data

The location of the combination band for different dioctahedral environments was predicted by adding up the corresponding wavenumbers of the δ(OH) and ν(OH) vibrations and converting the results to micrometers[2]. The δ(OH) wavenumbers correspond to scaled DFT results modeled for the Small Dimer clusters (Martínez-Alonso et al. 2002). The ν(OH) wavenumbers are those reported by Besson and Drits for mica-like environments (1997a). Experimental instead of calculated ν(OH) wavenumbers have been used to predict the location of the combination band because, as discussed earlier, these modeling results did not contemplate the effect on ν(OH) of apical O atoms of the tetrahedral sheet with unsatisfied charges. The locations of the predicted combination bands for OH in Al$_2$, AlMg, and AlFe^{3+} environments are equivalent to those observed in the SWIR spectra of our mineral samples and to assignments compiled from the literature (Table 5).

All our samples presented a well-developed band between 2.19 and 2.21 μm. It is commonly accepted that this combination band corresponds to the OH group surrounded by [VI]Al (Hunt et al. 1973; Bishop et al. 1999). The octahedral Al content in our samples and the location of this band show a distinct negative correlation ($R^2 = 0.56$). According to Besson and Drits (1997a), ν(Al$_2$OH) bands found at higher wavenumbers are only well developed in Al-rich samples. Therefore, combination bands occurring at shorter wavelengths (near 2.19 μm) would be found in [VI]Al-rich samples (Fig. 9). This agrees with observations made by Post and Noble (1993), Duke (1994), and Swayze (1997). Another explanation for having multiple

locations for Al-related combination bands was offered by Crowley and Vergo (1988) who studied the spectra of interlayered illite/smectite. They found that the OH combination band occurs near 2.22 μm in pure illite samples, and closer to 2.20 μm in pure smectite samples. This finding is in agreement with the observed larger ν(OH) wavenumbers in smectites than in mica-like minerals of the same octahedral composition (Fig. 6). The δ(OH) could also contribute to the variability observed in the 2.2 μm combination band: larger δ(OH) wavenumbers have been identified in species with mainly tetrahedral charge (e.g., beidellite, muscovite), as compared to those found in species with mainly octahedral charge (e.g., montmorillonite, phengite) (Petit, personal communication).

Samples with the highest octahedral Fe and Mg content present a second, less-well developed combination band in the 2.24–2.25 μm range. The AlFe^{3+} and AlMg OH-related fundamentals are usually broad and not as well developed as Al$_2$-related fundamentals. Consequently, AlFe^{3+} and AlMg combination bands in dioctahedral phyllosilicates usually translate into broad depressions in the right limb of the 2.2 μm combination band (Fig. 10), rather than into distinct absorption features. Moreover, their proximity to each other makes differentiation between the two very difficult. The presence or absence of these broad depressions may indicate the presence or absence of Mg and/or Fe^{3+} in the sample. The 2.2 μm band in samples without octahedral Mg and Fe^{3+} tend to have steep limbs. According to the wavenumbers of the ν(OH) and δ(OH) fundamentals in an AlFe^{3+} environment, their combination band should occur at 2.24–2.25 μm. Bishop et al. (1999) identified the AlFe^{3+} combination band at 2.237 μm in two Fe-rich smectites. The combination band in an AlMg environment is predicted to occur at 2.25 μm. Madejová et al. (2000) found in one smectite sample a combination band located at 2.239 μm that they identified as corresponding to an AlMg environment.

Combination bands corresponding to octahedral environments other than Al$_2$, AlMg, and AlFe^{3+}, have not been identified in our SWIR spectra, because these octahedral environments are not common in our samples. Spectra of glau-

---

[2] Because we now enter into the remote sensing domain (as opposed to the spectroscopy domain), a change in spectral units from cm^{-1} (wavenumber) to μm or nm (wavelength) is required, for historical reasons of general usage.

TABLE 4. Assignments of the bands identified in the SWIR analysis

Sample	OH combination band (μm)	
Guatemala	2.214	2.248
Ruby	2.193	(2.244)
Marshall Gulch	2.200	2.238
Tanzania	2.206	2.243
Isinglass	2.195	2.239
Capitan	2.205	2.241
Mt. Alamo	2.197	(2.231)
Pegma	2.195	2.235
Empire	2.195	–
Miller-Walters (I)	2.204	2.250
Tip Top	2.195	(2.247)
Miller-Walters (II)	2.197	2.251
Miller-Walters (III)	2.195	(2.250)
Phillips	2.193	–
Imt-1	2.206	2.255
AR1	2.206	(2.255)
LF7	2.197	–
RM3	2.200	(2.250)
RM6	2.197	–
RM8	2.197	–
RM11	2.192	–
RM21	2.197	–
RM22	2.191	–
RM30	2.197	–
RM31	2.203	–
RM35a	2.197	–
RM35c	2.195	(2.246)
RM35d	2.197	(2.254)
RM4	2.201	–
SG1	2.191	–
SG4	2.195	–
SilverHill	2.205	(2.253)
Marblehead	2.214	(2.249)
Fithian	2.204	2.255

Note: Location of less defined bands are shown in parenthesis.

TABLE 5. Scaled, modeled $\delta(OH)$, experimental $\nu(OH)$, and predicted and experimental wavelengths of their combination band in mica-like dioctahedral phyllosilicates as a function of the (MM') cationic environment of the hydroxyl group

MM'	$\delta(OH)$ (cm^{-1})	$\nu(OH)$ (cm^{-1})	Combination (μm) (predicted)	Combination (μm) (experimental)
Al$_2$	924 *	3658 †,	2.182 ‡,	2.2 §, 2.212 ‖,
		3641 †,	2.190 ‡,	2.19–2.21 **
		3621 †	2.200 ‡	
Al Fe^{3+}	876 *	3573 †	2.248 ‡	2.237 ‖, 2.24–2.25 **
Al Mg	840 *	3604 †	2.250 ‡	2.239 #, 2.24–2.25 **
Al Fe^{2+}	820 *	3559 †	2.284 ‡	–
Mg Fe^{3+}	796 *	3559 †	2.296 ‡	2.304 ‖
Fe$_2^{3+}$	833 *	3535 †	2.289 ‡	2.3 ††, 2.288 ‖
Fe^{2+} Fe^{3+}	808 *	3521 †	2.310 ‡	–
Mg$_2$	765 *	3583 †	2.300 ‡	–
Mg Fe^{2+}	754 *	3543 †	2.327 ‡	–
Fe$_2^{2+}$	691 *	3505 †	2.383 ‡	–

* Scaled DFT-DND wavenumbers modeled by Martínez-Alonso et al. (2002).
† Experimental values from Besson and Drits (1997a) in mica-like environments.
‡ Combination bands calculated in this study from (*) and (†).
§ Hunt et al. (1973).
‖ Bishop et al. (1999).
Madejová et al. (2000).
** This study.
†† Clark et al. (1993).

conites (Clark et al. 1993), and smectites (Bishop et al. 1999) with Fe$_2^{3+}$ octahedral occupancy, support the predicted location of the Fe$_2^{3+}$ combination band near 2.29 μm. A combination band due to MgFe^{3+} octahedral occupancy was identified by Bishop et al. (1999) in one smectite sample near 2.30 μm, close to our predicted value at 2.296 μm.

The intensity of these combination bands does not appear to be correlated with the abundance of Al, Mg, or Fe^{3+} in our samples. Other factors, such as particle size (Hunt 1977), may contribute to the intensity of these absorption bands.

Effect of interlayer cations on the OH combination band

The possibility of identifying the nature of interlayer cations in dioctahedral phyllosilicates such as smectites through the study of their IR spectra would be of great interest, since size and charge of interlayer cations in smectites determine important properties of these minerals, such as swelling potential (Moore and Reynolds 1997).

Ryskin (1974) described a reduction in $\nu(OH)$ wavenumbers in Ca-beidellite and Ca-montmorillonite (3553 cm^{-1} and 3533 cm^{-1}, respectively) when compared with talc and pyrophyllite, which lack interlayer cations (3678 cm^{-1}) and with phlogopite (3710–3720 cm^{-1}), which has potassium in the interlayer. We believe that these differences could be explained by the peculiarities of pyrophyllite (lack of layer charge), and the differences between di- and trioctahedral minerals already discussed. Farmer (1974) proposed interlayer cations as one of the factors affecting $\nu(OH)$ in trioctahedral micas, but not in dioctahedral

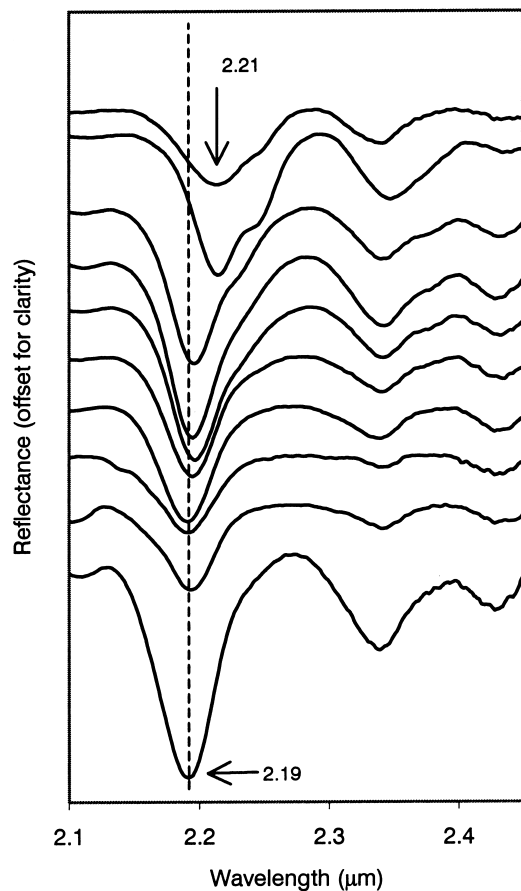**FIGURE 9.** Detail of some continuum-removed SWIR spectra of illite and muscovite, showing the relationship between location of the $\nu(OH)$ and $\delta(OH)$ combination band (near 2.2 μm) with abundance of octahedral Al. [VI]Al content increases from top to bottom.
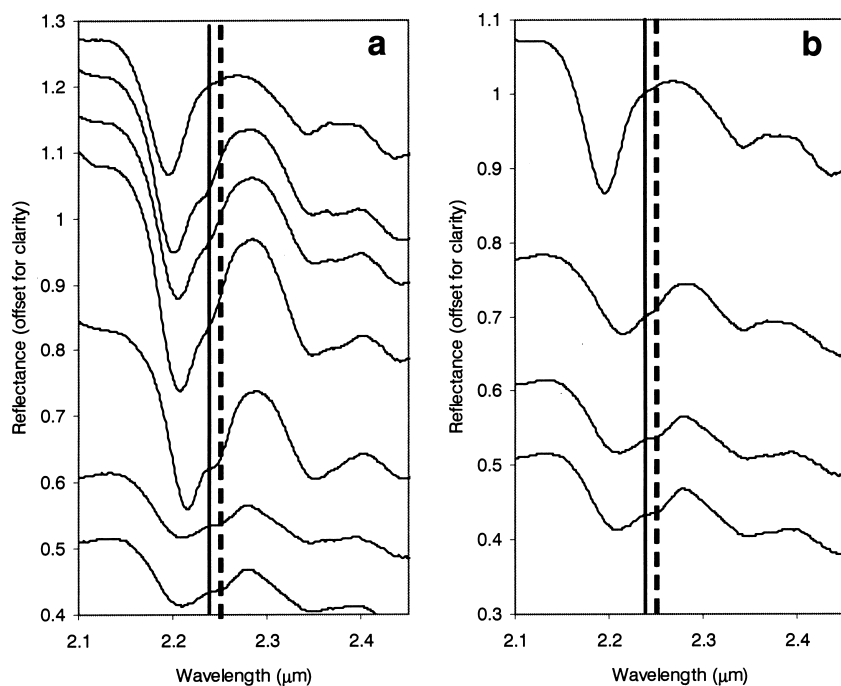
FIGURE 10. Detail of some SWIR spectra of dioctahedral phyllosilicates (illite and muscovite): $[VI]Fe^{3+}$-rich samples (**a**), $[VI]Mg$-rich samples (**b**). Vertical lines indicate the predicted location for the $AlFe^{3+}$ combination band, in the 2.24 (continuous line)–2.25 μm range, and the AlMg band at 2.25 μm (dashed line).

minerals. That would be justified by orientation of the hydroxyl group in trioctahedral environments, which minimizes the distance between interlayer cations and the hydrogen atom. Clark and co-authors (1990) observed shifts in the combination band of dioctahedral smectites from 2.204 to 2.214 μm, and found that the shifts were directly correlated with increasing Ca content in the interlayer. These authors pointed out that other factors could be affecting the band position, and proposed testing by cation substitution to verify their hypothesis.

To predict the effect of the nature of interlayer cations on the ν(OH) vibration, the SPEC scheme was applied to a geometrically constrained Dimer cluster, modified by adding interlayer cations in the position that they would occupy in muscovite (atomic coordinates from Rothbauer 1971). Again, the hydrogen atoms were oriented in the same way that they are on average in muscovite, inclined 15° with respect to the sheets. Only one type of Dimer $[Al_2 (OH)_2 (H_2O)_8]$ was modeled. K, Na, and Ca were selected as successive interlayer cations because they are the most common cations in the interlayer of phyllosilicates. The calculated energies, PES minimum, second derivatives of the PES at its minimum, and stretch wavenumbers are shown in Table 6. These results show that the effect of interlayer cation occupancy on ν(OH) is negligible, especially when taking into consideration the fact that in this setting that effect should be maximized, since the charge of the interlayer cation is neither shielded by a tetrahedral sheet nor shared with a second 2:1 layer.

The effect of interlayer cations on δ(OH) remains untested. Nevertheless, we may predict the following effect (if any) of the interlayer cation on the δ(OH) fundamental: A divalent cation (such as Ca) would repel more strongly the H in the hydroxyl group than a monovalent cation (such as Na or K). That would restrict the bend motion range of the OH group, increasing its frequency. The predicted effect of having a divalent cat-

ion in the interlayer, if any, would translate in a combination band located at shorter wavelengths.

These SPEC modeling results agree with experimental work done by Bishop et al. (1994), who studied FTIR spectra of montmorillonites, and by Brigatti et al. (1999), who analyzed montmorillonites and beidellites, interchanging the interlayer cations of these samples with Na and Ca among other elements. Their spectra showed no evidence of change in the local environment of the OH group after these treatments.

We conclude that interlayer cations per se most probably cannot affect the ν(OH) fundamental. We believe that shifts previously reported in the 2.2 μm combination band of smectites may be caused by octahedral substitution of Al by Mg, and/or by tetrahedral substitution, rather than by the nature of the

TABLE 6. SPEC results for modified Dimer clusters including interlayer cations

OH x^*	Interlayer Ca $E\,Al_2$ †	Interlayer Na $E\,Al_2$ †	Interlayer K $E\,Al_2$ †
0.82	−2588.013	−1561.236	−2434.816
0.84	−2588.031	−1561.255	−2434.835
0.86	−2588.046	−1561.270	−2434.850
0.88	−2588.057	−1561.281	−2434.861
0.9	−2588.066	−1561.290	−2434.870
0.92	−2588.073	−1561.297	−2434.877
0.94	−2588.077	−1561.301	−2434.881
0.96	−2588.080	−1561.304	−2434.884
0.98	−2588.081	−1561.305	−2434.885
1.00	−2588.081	−1561.305	−2434.885
1.02	−2588.079	−1561.303	−2434.883
1.04	−2588.077	−1561.301	−2434.881
1.10	−2588.064	−1561.288	−2434.868
1.20	−2588.033	−1561.257	−2434.837
x_{min} *	0.985	0.985	0.985
d^2E / dx^2 ‡	3.31480	3.32420	3.33042
$\bar{\nu}$ §	4939	4946	4950

* OH distance (x) and minimum OH distance (x_{min}) in angstroms.
† Energy (E) in Hartrees.
‡ d^2E/dx^2 is the second derivative of the PES at its minimum.
§ Wavenumber ($\bar{\nu}$) in cm^{-1}.

interlayer cations. It has been proposed, though, that in some smectites the position of the interlayer cation may vary accordingly to their hydratation state (Esposito et al. 1983). In the extreme case when the interlayer cation migrates through the siloxane surface to coordinate directly with the OH group, the fundamental modes of vibration of the hydroxyl will indeed be affected by that cation. Farmer (1974) refers to that effect, observed in dehydrated Ca- and Mg-saturated montmorillonite and beidellite with observed ν(OH) as low as 3500 cm^{-1}.

REFERENCES CITED

Badger, R.M. (1934) A relation between internuclear distances and bond force constants. Journal of Chemical Physics, 2, 128–131.
———(1935) The relation between the internuclear distances and force constants of molecules and its application to polyatomic molecules. Journal of Chemical Physics, 3, 710–714.
Besson, G. and Drits, V.A. (1997a) Refined relationships between chemical composition of dioctahedral fine-grained mica minerals and their infrared spectra within the OH stretching region. Part I: identification of the OH stretching bands. Clays and Clay Minerals, 45, 158–169.
———(1997b) Refined relationships between chemical composition of dioctahedral fine-grained mica minerals and their infrared spectra within the OH stretching region. Part II: The main factors affecting OH vibrations and quantitative analysis. Clays and Clay Minerals, 45, 170–183.
Bishop, J., Murad, E., Madejová, J., Komadel, P., Wagner, U., and Scheinost, A. (1999) Visible, Mossbauer and infrared spectroscopy of dioctahedral smectites: Structural analyses of the Fe-bearing smectites Sampor, SWy-1 and SWa-1. Proceedings 11th International Clay Conference. Ottawa, Canada, 413–420 (not seen; extracted from Clay Minerals, 35, 754, 2000).
Bishop, J.L., Pieters, C.M., and Edwards, J.O. (1994) Infrared spectroscopic analyses on the nature of water in montmorillonite. Clays and Clay Minerals, 42, 702–716.
Brigatti, M.F., Lugli, C., Montorsi, S., and Poppi, L. (1999) Effects of exchange cations and layer-charge location on cysteine retention by smectites. Clays and Clay Minerals, 47, 664–671.
Brindley, G.W. and Kao, C.C. (1984) Structural and IR relations among brucite-like divalent metal hydroxides. Physical Chemical Letters, 10, 187–191.
Burns, R.G. and Greaves, C.J. (1971) Correlation of infrared and Mössbauer site population measurements of actinolites. American Mineralogist, 56, 2010–2033.
Clark, R.N., King, T.V.V., Klejwa, M., and Swayze, G.A. (1990) High spectral resolution reflectance spectroscopy of minerals. Journal of Geophysical Research, 95, 12,653–12,680.
Clark, R.N., Swayze, G.A., Gallagher, A.J., King, T.V.V., and Calvin, W.M. (1993) The U.S. Geological Survey digital spectral library: Version 1: 0.2 to 3.0 microns. U.S. Geological Survey Open File Report 93–592, 1340 pages.
Crowley, J.K. and Vergo, N. (1988) Visible and near-infrared (0.4 to 2.5 μm) reflectance spectra of selected mixed-layer clays and related minerals. Proceedings International Symposium on Remote Sensing of the Environment. 6th Thematic Conference, Remote Sensing for Exploration Geology. Houston, Texas.
Duke, E.F. (1994) Near infrared spectra of muscovite, Tschermak substitution, and metamorphic reaction progress: Implications for remote sensing. Geology, 22, 621–624.
Esposito, G., Prost, R., and Gaultier, J.P. (1983) Infrared spectroscopy study of adsorbed water on reduced-charge Na/Li-montmorillonites. Clays and Clay Minerals, 31, 9–16.
Farmer, V.C. (1974) The layer silicates. In V.C. Farmer, Ed., The infrared spectra of minerals, p. 331–363. Mineralogical Society Monograph 4, London.
Gill, R. (1989) Chemical fundamentals of geology. Chapman and Hall, London, 291 p.
Hill, R.J., Craig, J.R., and Gibbs, G.V. (1979) Systematics of the spinel structure type. Physics and Chemistry of Minerals, 4, 317–339.
Hollas, J.M. (1996) Modern spectroscopy. 3rd edition. John Wiley and Sons. Chichester, 391 pp.
Hunt, G.R. (1977) Spectral Signatures of Particulate Minerals in the Visible and Near Infrared. Geophysics, 42, 501–513.

Hunt, G.R. and Salisbury, J.W. (1970) Visible and near-infrared spectra of minerals and rocks: I Silicate minerals. Modern Geology, 1, 283–300.
Hunt, G.R., Salisbury, J.W., and Lenhoff, C.J. (1973) Visible and near-infrared spectra of minerals and rocks: VI Additional silicates. Modern Geology, 4, 85–106.
Iishi, K. (1978) Lattice-dynamics of corundum. Physics and Chemistry of Minerals, 3, 1–10.
Madejová, J., Bujdák, J., Petit, S., and Komadel, P. (2000) Effects of chemical composition and temperature of heating on the infrared spectra of Li-saturated dioctahedral smectites. (II) Near-infrared region. Clay Minerals, 35, 753–761.
Martínez-Alonso, S., Rustad, J.R., and Goetz, A.F.H. (2002) Ab initio quantum mechanical modeling of infrared vibrational frequencies of the OH group in dioctahedral phyllosilicates. Part I: Methods, results and comparison to experimental data. American Mineralogist, 87, 1215–1234.
Moore, D.M. and Reynolds, R.C. (1997) X-ray diffraction and the identification and analysis of clay minerals, 2nd ed., 378 p. Oxford University Press, U.K.
Petit, S., Madejová, J., Decarreau, A., and Martin, F. (1999) Characterization of Octahedral Substitutions in Kaolinites Using Near Infrared Spectroscopy. Clays and Clay Minerals, 47, 103–108.
Post, J.L. and Noble, P.N. (1993) The near-infrared combination band frequencies of dioctahedral smectites, micas and illites. Clays and Clay Minerals, 41, 639–644.
Redhammer, G.J., Beran, A., Schneider, J., Amthauer, G., and Lottermoser, W. (2000) Spectroscopic and structural properties of synthetic micas on the annite-siderophyllite binary: Synthesis, crystal structure refinement, Mössbauer, and infrared spectroscopy. American Mineralogist, 85, 449–465.
Robert, J.L. and Kodama, H. (1988) Generalization of the correlations between hydroxyl-stretching wavenumbers and composition of micas in the system K_2O-MgO-Al_2O_3-SiO_2-H_2O: A single model for trioctahedral and dioctahedral micas. American Journal of Science, 288A, 196–212.
Rothbauer, R. (1971) Investigation of a 2M-muscovite with neutron rays. New Yearbook of the Mineralogy Monthly Journal, pp. 143–154 (in German).
Ryskin, Y.I. (1974) The vibrations of protons in minerals: hydroxyl, water and ammonium. In: The Infrared Spectra of Minerals. Farmer, V.C., editor. Mineralogical Society Monograph 4. London.
Sainz-Díaz, C.I., Timón, V., Botella, V., and Hernández-Laguna, A. (2000) Isomorphous substitution effect on the vibration frequencies of hydroxyl groups in molecular cluster models of the clay octahedral sheet. American Mineralogist, 85, 1038–1045.
Saksena, B.D. (1964) Infrared hydroxyl frequencies of muscovite, phlogopite and biotite micas in relation to their structures. Journal of the Chemical Society, Faraday Transactions, 60, 1715–1725.
Shannon, R.D. and Prewitt, C.T. (1969) Effective ionic radii in oxides and fluorides. Acta Crystallographica, B25, 925–946.
Slonimskaya, M.V., Besson, G., Dainyak, L.G., Tchoubar, C., and Drits, V.A. (1986) Interpretation of the IR spectra of celadonites and glauconites in the region of OH-stretching frequencies. Clay Minerals, 21, 377–388.
Strens, R.G.J. (1974) The common chain, ribbon and ring silicates. In V.C. Farmer, Ed., The Infrared Spectra of Minerals, p. 305–330. Mineralogical Society Monograph 4, London.
Štubičan, V. and Roy, R. (1961) Isomorphous Substitution and Infrared Spectra of the Layer Lattice Silicates. American Mineralogist, 46, 32–51.
Swayze, G.A. (1997) The hydrothermal and structural history of the Cuprite mining district, Southwestern Nevada: an integrated geological and geophysical approach, 341 p. Ph.D. dissertation, University of Colorado, Boulder.
Vedder, W. (1964) Correlations between infrared spectrum and chemical composition of mica. American Mineralogist, 49, 736–768.
Vedder, W. and McDonald, R.S. (1963) Vibrations of the OH Ions in Muscovite. Journal of Chemical Physics, 38, 1583–1590.
Velde, B. (1978) Infrared spectra of synthetic micas in the series muscovite-MgAl celadonite. American Mineralogist, 63, 343–349.
———(1983) Infrared OH-stretch bands in potassic micas, talcs and saponites; influence of electronic configuration and site of charge compensation. American Mineralogist, 68, 1169–1173.
Yang, K., Huntington, J.F., Boardman, J.W., and Mason, P. (1999) Mapping Hydrothermal Alteration in the Comstock Mining District, Nevada, Using Simulated Satellite-borne Hyperspectral Data. Australian Journal of Earth Sciences, 46, 915–922.
Yang, K., Browne, P.R.L., Huntington, J.F., and Walsheh, J.L. (2001) Characterising the hydrothermal alteration of the Broadlands-Ohaaki geothermal system, New Zealand, using short-wave infrared spectroscopy. Journal of Volcanology and Geothermal Research, 106, 53–65.
Wilkins, R.W.T. and Ito, J. (1967) Infrared study of some synthetic talcs. American Mineralogist, 52, 1649–1661.